In Vivo Albumin-Binding of a *C*-Functionalized Cyclam Platform for ^{64}Cu-PET/CT Imaging in Breast Cancer Model

Thomas Le Bihan,[1] Cathryn H. S. Driver,[2] Thomas Ebenhan,[2] Nathalie Le Bris,[1,*] Jan Rijn Zeevaart[2,*] and RaphaëlTripier[1,*]

[1] Univ. Brest, UMR CNRS 6521 CEMCA, 6 avenue Le Gorgeu, CS93837, 29200 Brest, France

[2] South African Nuclear Energy Corporation, Radiochemistry and NuMeRI PreClinical Imaging Facility, Elias Motsoaledi Street, R104 Pelindaba, North West, 0240, South Africa

ABSTRACT In the aim to design small molecules capable of binding *in vivo* to albumin to form bioconjugates, a second generation GluCAB derivative(Glucose-Chelator-Albumin Bioconjugate) has been synthesized and studied for *in vivo* ^{64}Cu-PET/CT imaging in breast cancer mice models together with its first-generation analogue. This series of radioligands - also capable of complexing therapeutic isotopes and therefore classified as theranostic agents - are working on the principle of tumor targeting through the Enhanced Permeability and Retention (EPR) effect as well as glucose metabolism. GluCAB-2^{Mal}, presented as an improved version of GluCAB-1^{Mal}, is a *C*-functionalized TE3A (1,4,8,11-tetraazacyclotetradecane-1,4,8-triacetate) containing a glucosyl moiety on its remaining secondary nitrogen atom and a *C*-functionalized linker terminating in a maleimide group for albumin capture. GluCAB-2^{NH_2} was used both as a "control" for *in vivo* studies and as the direct precursor of GluCAB-2^{Mal} and/or [^{64}Cu]Cu-GluCAB-2^{Mal}. The direct ^{64}Cu-radiolabeling of both GluCAB-2^{NH_2} and GluCAB-2^{Mal} (produced as a ready-to-label kit) was highly successful with 99% labeling efficiency (0.4 equiv [^{64}Cu]$CuCl_2$, 0.01M PBS buffer, 30 min, 45 °C). Both the amine and maleimide ^{64}Cu-labeled GluCAB derivatives exhibited high serum stability with [^{64}Cu]Cu-GluCAB-2^{Mal} binding almost immediately (> 95%) to serum proteins. *In vivo* experiments for the comparison of biodistribution and tumor targeting between [^{64}Cu]Cu-GluCAB-2^{NH_2}, [^{64}Cu]Cu-GluCAB-2^{Mal} and [^{64}Cu]Cu-GluCAB-1^{Mal} encompassed microPET/CT imaging and *post-mortem* biodistribution analysis in an allograft E0771 breast cancer mouse model. All three compounds exhibited hepatobiliary metabolism and excretion; however, while the amine-control compound was rapidly cleared from the blood, the two maleimide compounds indicated a prolonged biological half-life (6 - 8 h). Tumor uptake of [^{64}Cu]Cu-GluCAB-2^{Mal} was clearly evident in the microPET/CT images with 2 times and 4 times as much accumulation as compared to [^{64}Cu]Cu-GluCAB-1^{Mal} and [^{64}Cu]Cu-GluCAB-2^{NH_2} respectively, with a tumor to muscle ratio up to a maximum of 5 after 24 h. Further comparison of [^{64}Cu]Cu-Glu-CAB-2^{Mal} to [^{64}Cu]Cu-GluCAB-1^{Mal} indicated a decrease in liver accumulation and improvement on liver clearance for GluCAB-2^{Mal}. The second-generation GluCAB derivative, GluCAB-2^{Mal}, therefore demonstrates a clear advantage over the first GluCAB derivative for the development of an albumin-binding theranostic radioligand in terms of its ease of synthesis and radiolabeling, as well as exhibiting improved pharmacokinetics and tumor targeting capabilities.

INTRODUCTION

PET (Positron Emission Tomography) imaging, and especially PET linked to CT (computed tomography), has become the preferred technique for the diagnosis of numerous diseases such as cancers,[1] but also Alzheimer disease,[2] infection,[3] inflammation,[3]hypoxia[4]or thrombosis[5,6]. PET/CT imaging, which uses positron (β^+) emitting isotopes, has been found to have improved sensitivity and spatial resolution with shorter scan times over the previously used SPECT (Single Photon Emission Computed Tomography) imaging.[7] In clinical practice, the most widely used radioisotope is currently fluorine-18 incorporated into a glucose to form the diagnostic tracer, [^{18}F]-FDG (2-deoxy-2-(^{18}F)fluoro-D-glucose), for the functional imaging of highly metabolically active cells/tissues such as cancer.[8] However, the non-specific distribution of [^{18}F]-FDG to other organs with high energy demands, such as brain, muscles and brown fat, has led to focused research into the development of new agents – radiopharmaceuticals/radioligands – capable of targeting tumors with high specificity and exhibiting high clearance (metabolism and excretion) from the rest of the system. New radiopharmaceuticals designed for oncological purposes should also be specifically directed toward cancers cells to avoid unwanted radiation of healthy tissues and improve on over all patient dosimetry.[9] The design and investigation of specific targeting radioligands represents an increasing research area that includes many differing approaches such as immunotargeting, peptide-targeting or exploitation of the tumor microenvironment (Enhanced Permeability and Retention (EPR) effect).

While immunotargeting and peptide-targeting (radiolabeled antibodies or proteins/peptide specific to over-expressed cell surface receptors) are the most specific and common targeting techniques, they have certain drawbacks, which include a high radiation dose to non-target organs as a result of the very long biological half-life and hence circulation time as well as their relatively slow accumulation in the tumor.[10] These drawbacks also preclude the use of many radiolabeled antibodies for diagnosis since the most commonly used PET isotopes have

half-lives that are too short to be compatible with antibodies and the time required for their accumulation.

The EPR effect is another possible method to achieve a more targeted delivery of the radioligand with attached radionuclide.[11] To realize this kind of targeting, the radioligand must have a total molecular weight greater than 40 kDa and is therefore attached to macromolecule to form a bioconjugate. Above this threshold, the bioconjugated radioligand will accumulate in the tumor environment because of the highly vascularized but poorly organized epithelial system that allows a macromolecule to extravasate across the vascular wall into the tumor environment.[12,13] Such a radioligand, due to its size, will also generally avoid glomerular filtration by the kidneys and consequently have an prolonged biological half-life and therefore more time for tumor accumulation. The EPR effect is considered to be a "passive targeting" method that can be realized by using macromolecular agents based on polymers, nanoparticles or proteins.

Besides the EPR "passive" effect, the targeting of cancerous cells can be enhanced by introducing a small molecule as "active" targeting moiety on the radioligand. Small molecule active targeting, similar to immuno- and peptide-targeting, has high specificity for cell membrane receptors but generally exhibits faster *in vivo* target accumulation and better systemic clearance than the larger conjugates and is more non-immunogenic.[14] For this purpose, a glucose group can be anchored to the chelator. Cancer cells have a distinct glucose metabolism compared to healthy cells, a phenomenon known as the Warburg effect,[15] and as such, glycosylated compounds have been shown to have an increased accumulation within tumors through overexpressed glucose associated transporters (GLUT).[16,17,18] It is therefore possible that the targeting of the cancerous cells can be achieved in two successive steps. Firstly, the passive targeting assists with accumulation of the radioligand inside the tumor environment, where secondly, the active targeting moiety can then bind to cancerous cells by the recognition of its specific receptors.

Any targeting radioligand must, by definition, contain a radionuclide. Radiolabeling can be done covalently to the recognition moiety using organic isotopes such as carbon-11 or fluorine-18. However, these isotopes have very short half-lives (carbon-11 $t_{1/2}$ = 20 min and fluorine-18 $t_{1/2}$ = 110 min) and require complicated organic synthesis for their incorporation, which is not ideal. Radiolabeling using metal isotopes with more suitable half-lives is made much easier by conjugating the recognition moiety to a ligand able to complex the radionuclide.

Amongst the most common β^+ emitting metallic radionuclides, such as copper-64, gallium-68 and zirconium-89, the ^{64}Cu-isotope appears as the radiometal of choice to perform PET imaging ($t_{1/2}$ = 12.7 h, β^+ 17.4%, E_{max} = 0.656 MeV, β^- 39.6%, E_{max} = 0.573 MeV). It has a low positron E_{max} providing a good image resolution and a half-life more suited for longer biological phenomena.[19] Although copper-64 can also be considered as a radionuclide with application for radiotherapy thanks to its β^- emissions, and is gaining more use within this field, the ^{67}Cu-isotope remains a more suitable isotope for this purpose as a pure β^- emitter with a longer half-life ($t_{1/2}$ = 62.0 h, β^- 100%, E_{max} = 0.577 MeV).[20] Therefore, ^{64}Cu and ^{67}Cu arise as a promising theranostic pair especially tailored for personalized medicine.

Beside the targeting requirements for a radiopharmaceutical, the *in vivo* use of a copper radionuclides, as for other cationic radiometals, requires the chelation of the radionuclide by an appropriate ligand able to form a thermodynamically stable and kinetically inert complex.[21,22] The stability of the complex is required to avoid the transchelation by metalloproteins leading to an unfavorable biodistribution in non-target organs and a decreased tumor uptake.[22] To this end, many chelating agents are under investigations, currently being applied in preclinical/clinical trials or already FDA approved. Amongst these, *N*-functionalized polyazacycloalkanes with coordinating acetate arms, such as NOTA (1,4,7-triazacyclononane-1,4,7-triaceticacid), DOTA (1,4,7,10-tetraazacyclododecane-1,4,7,10-tetraaceticacid), and TETA (1,4,8,11-tetraazacyclo tetradecane-1,4,8,11-tetraacetic acid), are widely used thanks to their exceptional coordinating properties (Figure 1).

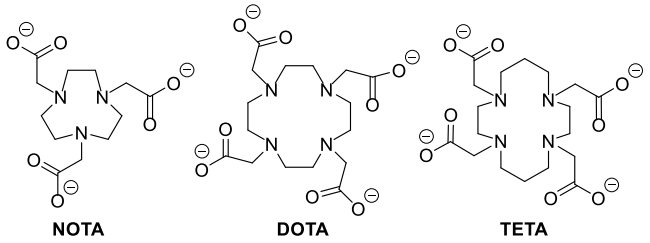

Figure 1. Structure of NOTA, DOTA and TETA

In previously published work, a similar tetraazamacrocycle was modified by two additional *N*-functionalized targeting groups to obtain GluCAB-1^{Mal} (glucose-chelator-albumin bioconjugate) (Figure2).[23] The proposed theranostic precursor agent is a chelating macrocycle functionalized with an active targeting glucosyl moiety and an alkyl linker terminating in a maleimide group that, after binding *in vivo* to circulating endogenous human serum albumin (HSA), furnishes the full active GluCAB bioconjugate, efficient for an initial accumulation via the EPR effect. HSA is the most abundant serum protein, its molecular weight is 66.5 kDa and its half-life is 19 days making it very stable in the context of an EPR effect agent.[24] Additionally, HSA is currently used as a protein carrier in the development of new targeting agents and albumin based macro-aggregates are already approved by the FDA for use in cancer treatments.[25,26,27] A common way to attach a small molecule to albumin is through a Michael addition of a maleimide to the free thiol group of the cysteine found in position-34 of the protein.[24,25]

For copper complexation, the cyclam backbone was selected as the most appropriate since the cavity is better suited for this cation with highly stable and inert complexes being formed;[28,29] it also appeared to be the most tunable platform considering all the recent successful studies in ^{64}Cu-PET imaging using cyclam-based chelators.[30,31,32,33,34,35] The approach to Glu-CAB-1^{Mal} was to use the cyclam platform functionalized with two acetate arms, namely TE2A. Although other cyclam derivatives have proved to be more suitable for the application, TE2A presented the advantage of being a decent copper(II) chelator,[36] while offering two remaining secondary amines that could be functionalized (Figure 2) for passive and active targeting.[37] Furthermore, the synthesis of TE2A is rather simple and well-described in literature.[34]

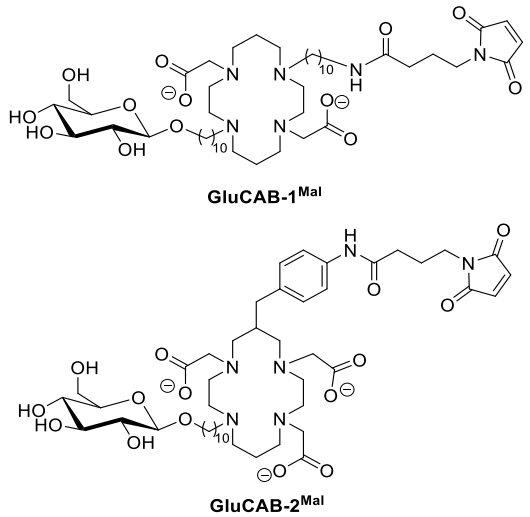

Figure 2. Structure of TE2A-chelator based GluCAB-1^{Mal} and of the envisaged TE3A-chelator based GluCAB-2^{Mal}

However, access to GluCAB-1^{Mal} was not simple, the secondary amine functions of the TE2A precursor (its *tert*-butyl diester derivative) being equivalent. A delicate statistical functionalization of these latter amines with the targeting groups was required leading to difficult purifications and poor yields. Nevertheless, the radiolabeling of this ligand with copper-64 was accomplished with high labeling efficiency and radiochemical purity (>98%) and the *in vivo* behavior of the [^{64}Cu]Cu-GluCAB-1^{Mal} was quite attractive showing a binding to circulating albumin by microPET/CT imaging and biodistribution analysis in healthy mice (biological half-life of 6 - 8 h) as compared to the control [^{64}Cu]Cu-GluCAB-1^{NH_2}.

Besides the challenging synthesis of GluCAB-1^{Mal}, other limitations included the radiolabeling conditions in acidic medium at a high temperature with prolonged heating ([^{64}Cu]$CuCl_2$; 0.1M NH_4OAc; pH 3.5; 90˚C; 30 min) that are not compatible with all applications. Additionally, while most of [^{64}Cu]Cu-GluCAB-1 was excreted after 24 hours, a high liver activity indicated potential release of free ^{64}Cu ions from the complex or transchelation to metalloenzymes. An alternative consideration for the high liver activity was that the neutral charge of the complex was delaying metabolism and excretion as compared to a negatively charged complex.[38]

These findings urged improvements to be made to the ligand design to achieve milder radiolabeling conditions as well as a negatively charged and more inert radiocomplex. Consequently, GluCAB-2^{Mal} (Figure 2) was envisaged - a more sophisticated cyclam platform capable of being more easily modified as compared to GluCAB-1^{Mal} - to address the limitations of the original structure.

Therefore, presented here is the efficient synthesis of GluCAB-2^{Mal} based on an alternative, more convenient design approach to macrocycle functionalization as previously described for the synthesis of protected *C*-functionalized cyclams with one additional grafting aniline moiety.[39,40] GluCAB-2^{Mal} was synthesized from a tri-acetate cyclam derivative bearing a para-aminobenzyl group on one carbon atom in a single β-*N* position of the macrocycle,[40,41] namely aniline-TE3A. This macrocycle was expected to lead to a faster radiolabeling, an increased stability and inertness and a negatively charged complex compared to TE2A. Additionally, the aniline-TE3A scaffold allowed for easy introduction of the targeting functions onto the single available secondary amine of the cyclam or onto the primary amine of the aniline group.

Following the synthesis and radiolabeling of GluCAB-2^{Mal}, the *in vivo* characterization of [^{64}Cu]Cu-GluCAB-2^{Mal} is further reported herein and included microPET/CT imaging and biodistribution studies in a murine breast cancer allograft mouse model. The corresponding non-conjugable amine precursor of GluCAB-2^{Mal}, called GluCAB-2^{NH_2}, was used as a control to provide a comparison for highlighting the albumin conjugation. Furthermore, the tumor-targeting potential of the previously synthesized [^{64}Cu]Cu-GluCAB-1^{Mal} was also investigated in this same rodent cancer model in order to provide a complete comparison of the two GluCAB derivatives to each other, and these results are detailed.

RESULTS AND DISCUSSION

Synthesis of GluCAB-2

The synthesis of GluCAB-2 requires the full control of the regiospecific *N*-functionalization of the *C*-functional cyclam core. In a previous work, we reported the synthesis of the *N*-benzylated *p*-NH_2-Bn-cyclam **1**.[41] This compound can be considered as a mono-*N*-protected, *C*-functionalized cyclam that is a valuable precursor for the tri-*N*-alkylation of the remaining secondary nitrogen atoms. The first step of the synthesis consists of the alkylation of the three secondary nitrogen atoms of compound **1**with *tert*-butylbromoacetate as precursor of the acetate functions (Scheme 1). The alkylation was performed at low temperature with a slight default of the electrophilic reagent to avoid, as much as possible, the alkylation of the less reactive primary amine of the aniline function. The reaction was followed by mass spectroscopy until the appearance of a small quantity of the tetra-*N*-alkylated product. The reaction mixture was purified by column chromatography to obtain compound **2** with a good yield (58%). The benzyl group of **2** was then removed by catalytic hydrogenolysis to quantitatively give the tri-*N*-alkylated compound **3** with only one secondary nitrogen atom available for a further functionalization. Characterization data and spectroscopic spectra for each intermediate are given in the SI. In order to introduce the glycosylated function on the cyclam core of **3**, we chose 10-bromodecyltetra-*O*-benzoyl-β-D-glucopyranoside previously described.[42] Because of the weak reactivity of this reagent due to the fatty chain, the nucleophilic substitution reaction had to be performed in CH_3CN under reflux for four days but, even in these harsh conditions, the nitrogen atom of the aniline was not alkylated. Glycosylated compound **4** was obtained after purification by column chromatography (Al_2O_3; $CHCl_3$/MeOH 100:0 to 95:5) with a good yield (68%). The subsequent one-pot removal of both acetate and benzoyl groups of **4** was performed in a mixture of aqueous KOH (1M) and EtOH (1:1). The purification of the crude product on reverse phase C18 HPLC led with 50% yield to the direct "amino" precursor of GluCAB-2^{Mal} that is noted as GluCAB-2^{NH_2}. The overall yield of the synthesis was satisfying with 19% over 4 steps. The subsequent step involving the linkage of the maleimide group leading to GluCAB-2^{Mal} would be investigated and performed at the last moment due to its previously described sensitivity, especially towards nucleophiles.

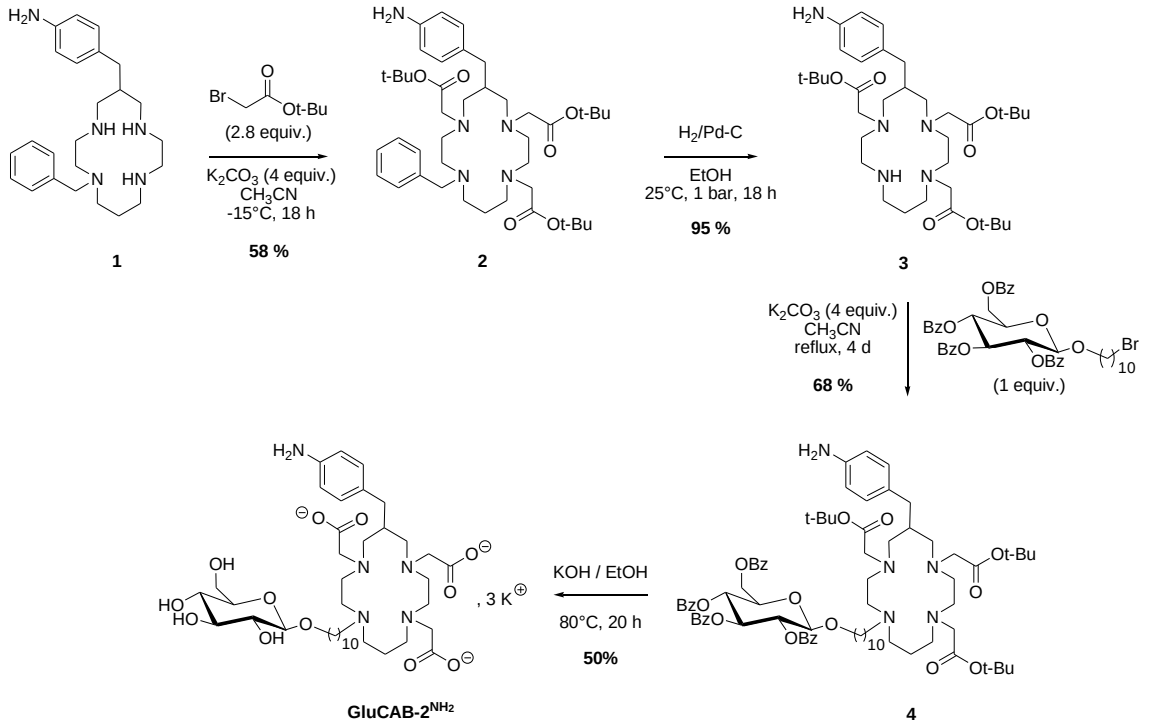

Scheme 1. Synthesis of GluCAB-2^{NH_2}, the direct "amino" precursor of GluCAB-2^{Mal}

Radioligand preparation, stabilities and protein binding

^{64}Cu-labeling of GluCAB-2^{NH_2}

In order to determine optimal ^{64}Cu-labeling conditions for the newly synthesized and designed radioligand, it was firstly decided to radiolabel GluCAB-2^{NH_2} with [^{64}Cu]$CuCl_2$ (1 equiv) as a model, according to the method used for GluCAB-1^{NH_2} with an incubation time of 30 minutes in a 0.1M NH_4OAc buffer at pH 3.5 at 90 °C. Under these conditions this ligand was radiolabeled quantitatively (99% labeling efficiency (LE) and radiochemical purity (RCP)). Subsequent ^{64}Cu-radiolabeling experiments were performed in a 0.01M PBS buffer at pH 7.4 to determine the success of the GluCAB-2 design for milder labeling conditions as compared to GluCAB-1. Radiolabeling of GluCAB-2^{NH_2} in the PBS buffer at 45 °C for only 20 minutes yielded the same results (99% LE and RCP), thereby proving that GluCAB-2 allows for radiolabeling in mild and physiologically suitable conditions.

Maleimide coupling reaction

Two approaches were considered to obtain the radiocomplex [^{64}Cu]Cu-GluCAB-2^{Mal} from GluCAB-2^{NH_2}. Method A (post-labeling conversion) consisted of first carrying out ^{64}Cu-labeling of GluCAB-2^{NH_2} and then coupling with maleimide derivative (4-maleimidobutyric acid NHS-ester), whereas method B (pre-labeling conversion) involved the two steps in the reverse order, first grafting of the maleimide and then radiolabeling (Scheme 2). The two approaches were investigated to determine the ease of maleimide coupling and the sensitivity of the maleimide to the milder PBS radiolabeling conditions. The [^{64}Cu]$CuCl_2$ radiolabeling of GluCAB-2^{NH_2} with respect to method A was easily performed in PBS as previously described, in mild conditions and in a wide pH range, to lead to [^{64}Cu]Cu-GluCAB-2^{NH_2}. Unfortunately, all attempts to proceed to the complete grafting of the maleimide derivative failed and a maximum conversion of 60% from [^{64}Cu]Cu-GluCAB-2^{NH_2} to [^{64}Cu]Cu-GluCAB-2^{Mal} was obtained. Method A was therefore deemed inappropriate for continuation to further *in vivo* experiments.

Method B was then investigated that started with the condensation reaction between GluCAB-2^{NH_2} and the maleimide derivative. The optimized reaction performed in a PBS buffer at 45 °C was monitored by following the reaction at room temperature in a NMR tube using ^{1}H NMR spectroscopy (Figure 3, left). The ^{1}H NMR spectroscopy followed the disappearance of the two doublets corresponding to the equivalent aromatic protons of the aniline group of GluCAB-2^{NH_2} in favor of the two new doublets of GluCAB-2^{Mal}. The integration of these signals allowed for estimating that 90% of GluCAB-2^{NH_2} was converted to GluCAB-2^{Mal} after incubation for 90 minutes. The crude product obtained from the reaction at 45 °C was purified through a solid phase extraction (SPE) C18 cartridge using 50% ethanol in water. GluCAB-2^{Mal} was then dried, dissolved again in the appropriate amount of PBS and lyophilized pending further use.

^{64}Cu-labeling of GluCAB-2^{Mal} using [^{64}Cu]$CuCl_2$ (0.4 equiv) was performed in a PBS buffer for 30 minutes at 45 °C. The radio-HPLC chromatogram (Figure 3, right) showed that [^{64}Cu]Cu-Glu-CAB-2^{Mal} represents approximately 90% of the radioactivity (blue peak) compared to some remaining unconverted [^{64}Cu]Cu-GluCAB-2^{NH_2} (green peak) with less than 4% of the total radioactivity. The red area between these two peaks

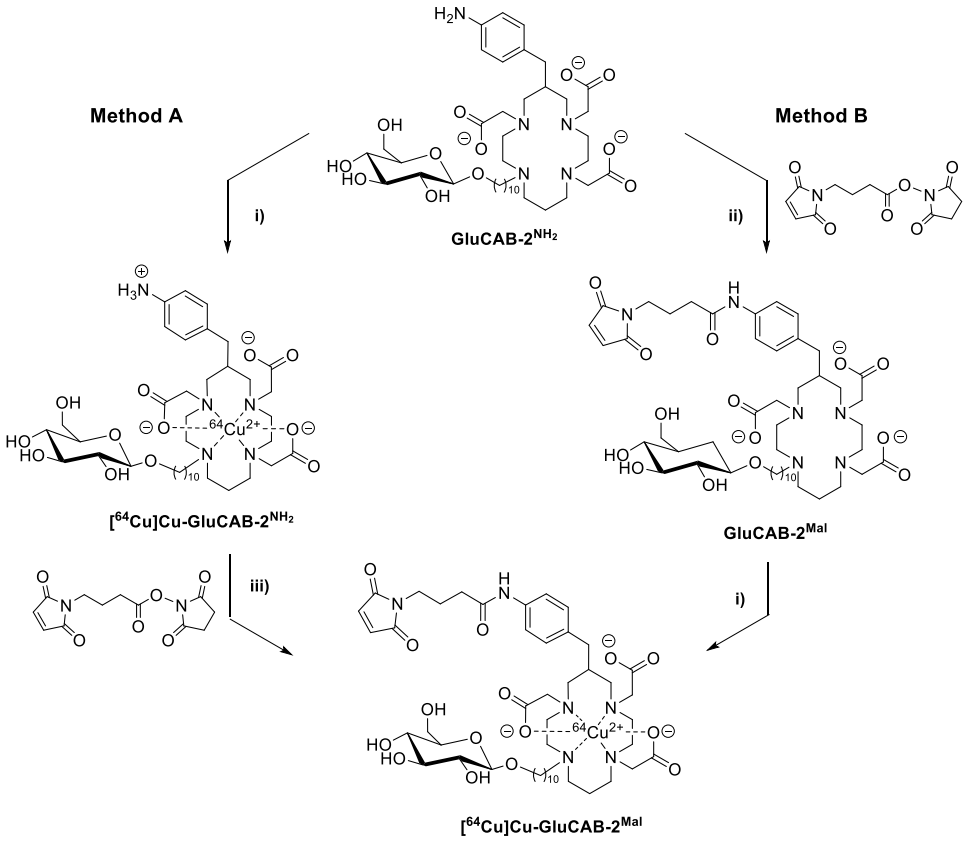

Scheme 2. Methods A and B used to synthesize [^{64}Cu]Cu-GluCAB-2^{Mal}; i) [^{64}Cu]$CuCl_2$ (0.4 equiv), 0.01M PBS, 45 °C, 30 min; ii) NHS-Maleimide (5 equiv) in DMF, 0.01M PBS, 45 °C, 90 min; iii) NHS-Maleimide (2 equiv), 0.01M PBS, 45 °C, 90 min.

can be attributed to a compound in which the maleimide function has been hydrolyzed. Nevertheless, the radio-HPLC chromatogram showed no trace of free ^{64}Cu-activity in the sample, evidence of the quantitative radiolabeling in these conditions, even after the maleimide moiety coupling.

The synthesis of GluCAB-2^{Mal} followed by ^{64}Cu-radiolabelling under mild physiological conditions facilitates the production of this radioligand as a "ready-to-label", one vial kit. This constitutes a clear advantage compared to GluCAB-1^{Mal} but also to several existent radioligands in terms of future development of the compound for clinical use.

EDTA challenge of [^{64}Cu]Cu-GluCAB-2^{NH_2}

Copper-64 has been proven to form highly stable and inert complexes with cyclam derivatives; however, this property still needs to be investigated for any new complexes. The kinetic inertness and thermodynamic stability of the [^{64}Cu]Cu-Glu-CAB-2^{NH_2} complex was therefore evaluated by determining the extent of isotope transchelation with 5 times and 25 times molar excess of ethylenediaminetetraacetic acid (EDTA) in 0.01 M PBS at pH 7 over 2 h at room temperature. [^{64}Cu]Cu-GluCAB-2^{NH_2} proved to be completely stable over this time period and no formation of [^{64}Cu]Cu-EDTA was noted.

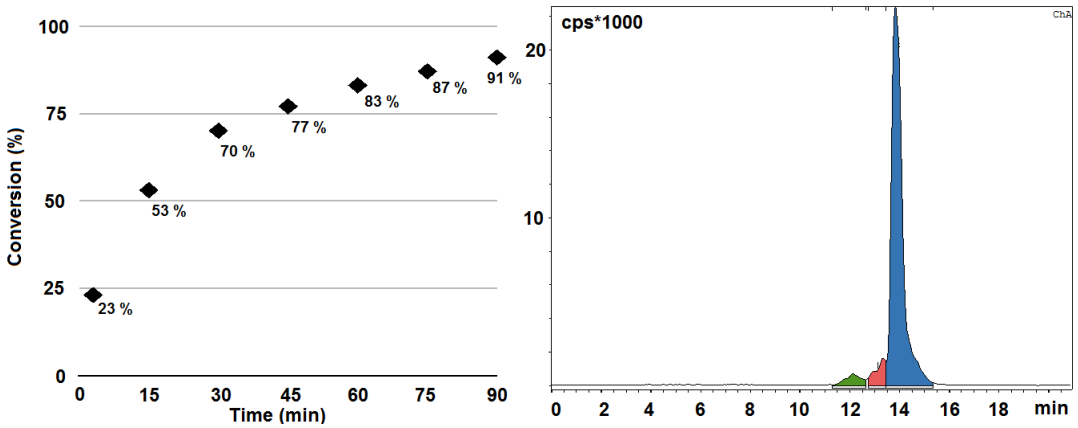

Figure 3. ^{1}H NMR spectroscopic monitoring of maleimide coupling reaction on GluCAB-2^{NH2} (left). Radio-HPLC chromatogram of [^{64}Cu]Cu-GluCAB-2^{Mal} (right).

Protein binding and serum stability of [^{64}Cu]Cu-GluCAB-2^{NH_2} and [^{64}Cu]Cu-GluCAB-2^{Mal}

[^{64}Cu]Cu-GluCAB-1^{Mal} was previously reported to be about 90% protein bound and exhibited high serum stability over 24 h at 37 ˚C.[23] These results were in line with the design of the compound to include the maleimide functionality for *in vivo* albumin-binding. The protein binding and serum stability studies were replicated for [^{64}Cu]Cu-GluCAB-2^{NH_2} and [^{64}Cu]Cu-Glu-CAB-2^{Mal}. The ^{64}Cu-compounds were incubated in human serum at 37 °C for 24 h with sampling and analysis done immediately after addition of the tracers to the serum as well as at 1, 2 and 24 h after addition (Figure 4).

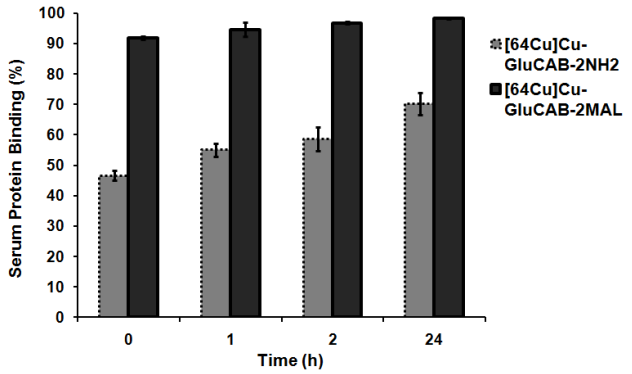

Figure 4. Serum Protein binding analysis for [^{64}Cu]-GluCAB-2^{NH_2} and [^{64}Cu]Cu-GluCAB-2^{Mal} over 24 h.

Similarly to [^{64}Cu]Cu-GluCAB-1^{Mal}, [^{64}Cu]Cu-GluCAB-2^{Mal} was rapidly bound to serum proteins (92%) and exhibited 98% binding after the 24 h period confirming the anticipated protein binding as a result of the maleimide group. Interestingly, although some protein binding as a result of non-specific protein interactions was expected for [^{64}Cu]Cu-GluCAB-2^{NH_2} since the amine precursor of GluCAB-1 exhibited 30% binding, the percentage [^{64}Cu]Cu-Glu-CAB-2^{NH_2} that was protein bound (45 – 70% in 24 h) was much higher than expected. The possible non-specific protein interactions include hydrogen bonding, hydrophobic interactions and charge interactions. The charge interactions are the most likely cause of increased protein binding for [^{64}Cu]Cu-GluCAB-2^{NH_2} since the terminal amine would be protonated under physiological conditions, but also the improved GluCAB-2 chelator contains a third acetate arm (negatively charged) which does not participate in isotope complexation and is therefore accessible for non-specific binding. The serum stability analysis for [^{64}Cu]Cu-GluCAB-2^{NH_2} indicated excellent ligand robustness and complex stability in serum over the 24 h period as no increase in free copper-64 or complex degradation products was noted. The majority of [^{64}Cu]Cu-Glu-CAB-2^{Mal} was protein bound which precluded serum stability analysis for ligand degradation products; however, no increase in free copper-64 was noted thereby indicting stability of the complex to demetallation.

***In vivo* experiments in tumor mice**

Previous *in vivo* studies (microPET/CT imaging and biodistribution in healthy mice) using [^{64}Cu]Cu-GluCAB-1^{Mal} and [^{64}Cu]Cu-Glu-CAB-1^{NH_2} as a control confirmed the prolonged biological half-life (6 – 8 h) of the compound, afforded by binding of the maleimide, to albumin *in vivo*.[23] These results also indicated an increased liver accumulation and slow excretion through the hepatobiliary pathway; however, most of [^{64}Cu]Cu-GluCAB-1^{Mal} was excreted within 24 h. The design of GluCAB-2^{Mal}, besides synthesis and radiolabeling challenges, was aimed at addressing the *in vivo* limitations of GluCAB-1^{Mal} by providing a stable, negatively charged complex to improve liver clearance and furthermore provide good tumor targeting.

[^{64}Cu]Cu-GluCAB-2^{Mal} and [^{64}Cu]Cu-GluCAB-2^{NH_2} (Figure 5) as the control were investigated in syngeneic (allograft tumor model) mice to confirm the ability of the maleimide to bind albumin *in vivo* and to evaluate tumor targeting through the EPR effect. Simultaneously, the capacity of the glucose moiety alone to target tumor cells would be evaluated. These results were then compared to the tumor targeting capability of [^{64}Cu]Cu-GluCAB-1^{Mal} in the same syngeneic mouse model.

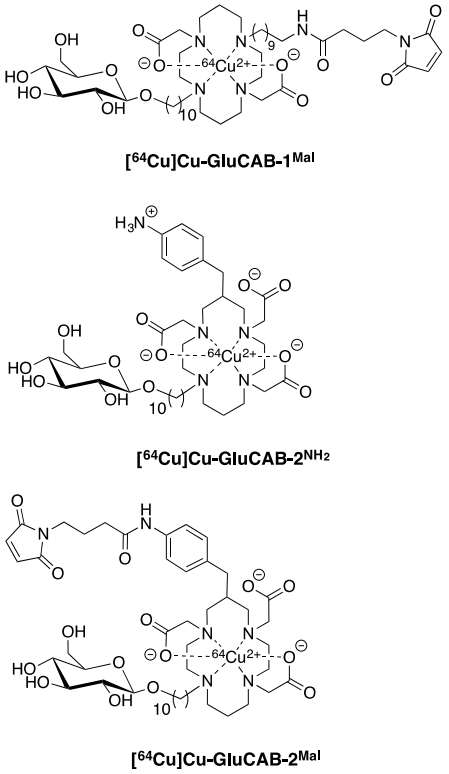

Figure 5. Structure of the radiopharmaceuticals used for *in vivo* studies (top: [^{64}Cu]Cu-GluCAB-1^{Mal}; bottom left: control [^{64}Cu]Cu-GluCAB-2^{NH_2}; bottom right: [^{64}Cu]Cu-GluCAB-2^{Mal}).

A syngeneic (allograft), orthotopic tumor mouse model is developed by growing mouse tumor cells in the same tissue of origin and in the same strain of immune-competent mice from which the tumor originated.[43] The advantages of using an allograft tumor model include cost-effectiveness, effortless implantation and more reproducible experimental tumor histology and growth rate.[44] The orthotopic allograft model used for this study was C57/BL6 mice inoculated with E0771 murine breast cancer cells into the mammary fat pad. The E0771 cell line has been commonly used for modelling of breast cancer,[45] as an elegant model for the measurement of glucose uptake and has demonstrated growth in fat pads of tumors that are highly vascularized

(a prerequisite to study EPR effect);[46,47] i.e. it will provide an effective model for proof of principal for possible tumor targeting using the GluCAB compounds.

PET imaging studies

Intravenous administration of [^{64}Cu]Cu-GluCAB-1^{Mal}, [^{64}Cu]Cu-GluCAB-2^{Mal} and [^{64}Cu]Cu-GluCAB-2^{NH_2} (7-10 MBq; ± 20 nmol) to E0771 allograft C57/BL6 mice resulted in no adverse effects and sequential microPET/CT imaging of the injected mice was conducted over a 24 h period. Maximum intensity projection (MIP) images at 1, 2, 6 and 24 h allowed for a visual comparison of the biodistribution of the three ^{64}Cu-compounds (Figure 6) while standard uptake values (SUV (g/mL)) and volumes-of-interest (VOI) provided image-guided quantification of the activity in the organs for all three compounds and allowed for time-activity-curves to be drawn (Figure7). The data for the control, [^{64}Cu]Cu-GluCAB-2^{NH_2}, indicated rapid metabolism and excretion of the compound through the liver with high activity seen in the gallbladder and intestines within 6 h post-injection (p.i.) (max SUV ~5-6 g/mL at 1-2 h p.i.). As expected, no tumor accumulation of [^{64}Cu]Cu-GluCAB-2^{NH_2} was visible at any point and at 24 h p.i. most of this compound was systemically cleared by the animal.

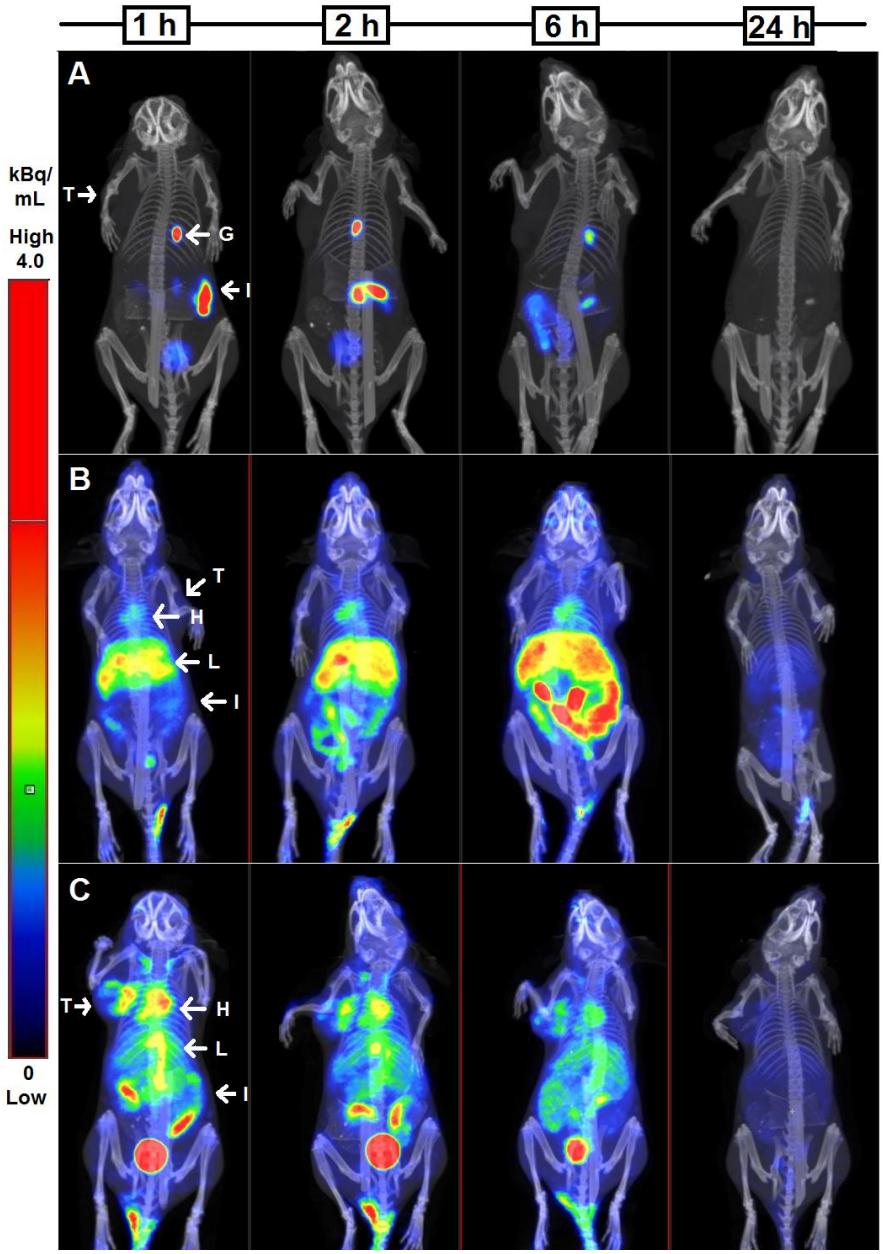

Figure 6: Representative Maximum Intensity Projection microPET/CT images of E0771 breast cancer allograft C57/BL6 mice following injection with (**A**) [^{64}Cu]Cu-GluCAB-2^{NH_2}, (**B**) [^{64}Cu]Cu-GluCAB-1^{Mal} and (**C**)[^{64}Cu]Cu-GluCAB-2^{Mal} at 1, 2, 6, and 24 h post-injection (n = 3). (T = E0771 tumor; H = heart; L = liver; G = gall bladder; I = intestines). Normalized scale bar 0 – 4 kBq/mL

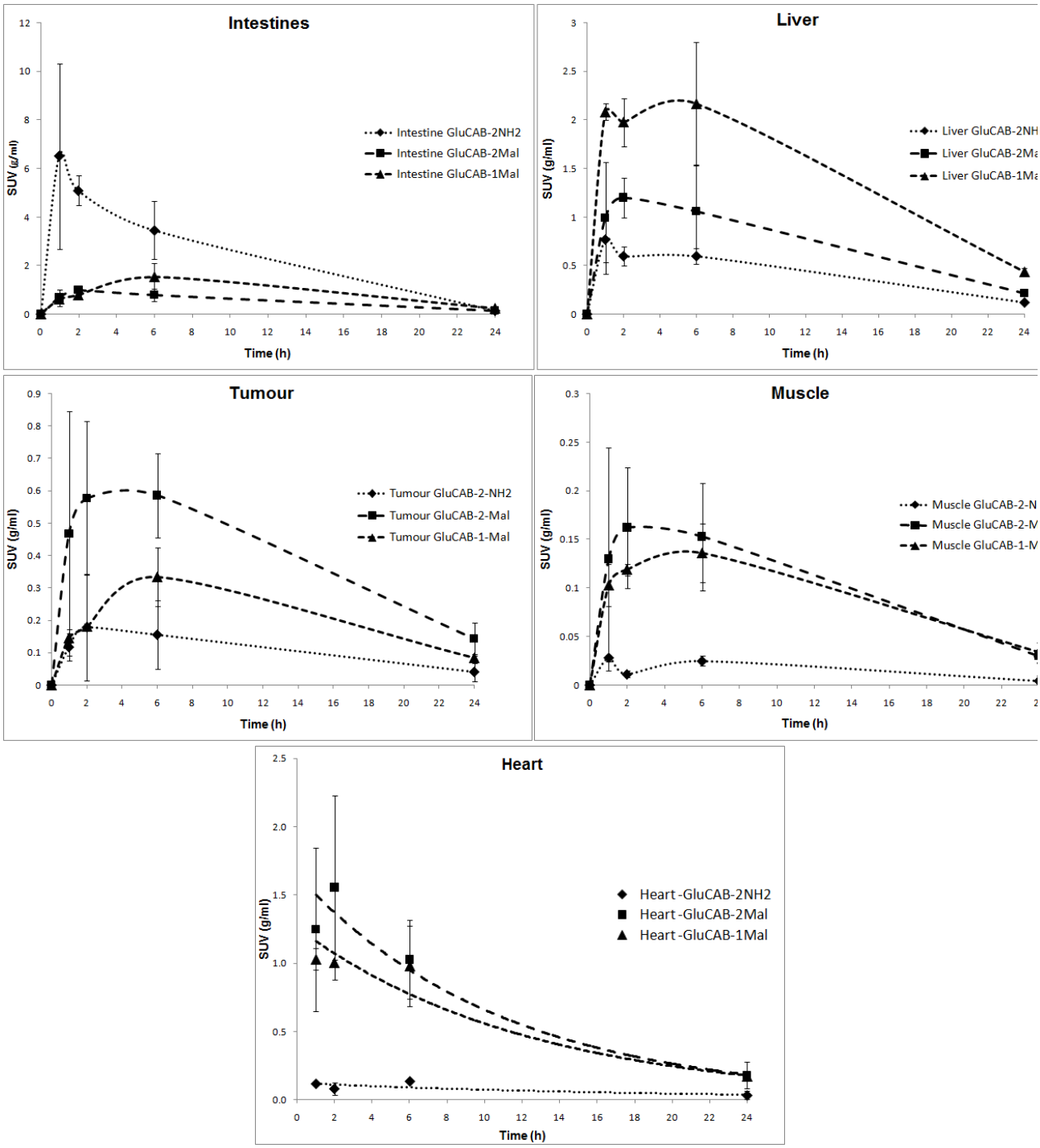

Figure 7: Time-activity-curves for the organs of interest (intestines, liver, heart, tumor and muscle) over 24 h period derived from SUV (g/mL) and VOI-analysis of sequential micro-PET/CT images of E0771 tumor bearing mice (n = 3) injected with (♦) [^{64}Cu]Cu-GluCAB-2^{NH2}, (▲) [^{64}Cu]Cu-GluCAB-1^{Mal} and (■) [^{64}Cu]Cu-GluCAB-2^{Mal}. Results are expressed as mean ± standard deviation.

[^{64}Cu]Cu-GluCAB-1^{Mal} and [^{64}Cu]Cu-GluCAB-2^{Mal} MIP images revealed a high presence of the compounds in the cardiovascular system (clear visualization of the myocardium) and analysis of the blood pool indicated an exponential decrease of the circulating activity over time with the biological half-life for [^{64}Cu]Cu-GluCAB-1^{Mal} and [^{64}Cu]Cu-GluCAB-2^{Mal} calculated to be between 6 – 8 h which is corresponding to results of previous study regarding the [^{64}Cu]Cu-GluCAB-1^{Mal} pharmacokinetics in healthy mice. A much slower metabolism and excretion through the liver and intestines was noted for [^{64}Cu]Cu-GluCAB-1^{Mal} and [^{64}Cu]Cu-GluCAB-2^{Mal} with SUV values of approximately 2 g/mL and 1 g/mL in the liver, respectively between 2 – 6 h p.i. The [^{64}Cu]Cu-GluCAB-2^{Mal} exhibited

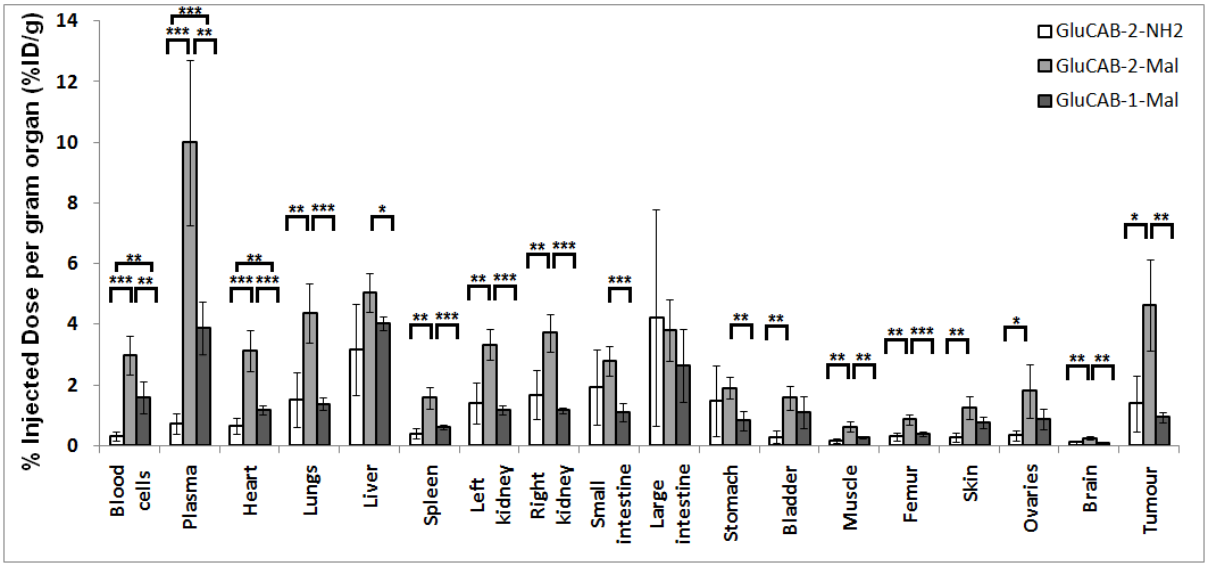

Figure 8: Comparison of the *ex vivo* biodistribution of [^{64}Cu]Cu-GluCAB-2^{NH2}, [^{64}Cu]Cu-GluCAB-2^{Mal} and [^{64}Cu]Cu-GluCAB-1^{Mal} in E0771 allograft C57/BL6 mice at 24 h p.i. (Data is presented as an average % ID/g for 5 animals ± SD)(*** = $p < 0.001$; ** = $p < 0.01$; * = $p < 0.05$)

significantly lower liver accumulation than [^{64}Cu]Cu-GluCAB-1^{Mal} at all-time points ($p < 0.05$, except at 6 h, $p = 0.07$). A significant organ washout ($p < 0.05$) from 6 h to 24 h was noted for all organs although the [^{64}Cu]Cu-GluCAB-1^{Mal} activity remaining in the liver at 24 h was still significantly higher ($p < 0.01$) than the [^{64}Cu]Cu-GluCAB-2^{Mal}. The activity in the muscle for all three compounds was minimal (SUV < 0.15) although a significant difference ($p < 0.05$) was still noted between the experimental groups and the control group as a result of higher activity remaining in the blood pool. A clear visual difference was seen between the tumor uptake of [^{64}Cu]Cu-GluCAB-1^{Mal} and [^{64}Cu]Cu-GluCAB-2^{Mal}. Whilst [^{64}Cu]Cu-GluCAB-1^{Mal}-microPET/CT showed minimal tracer accumulation, the tumors of mice following [^{64}Cu]Cu-GluCAB-2^{Mal}-microPET/CT were clearly delineated from background radioactivity as early as 1 h p.i. with the maximum tissue concentration (0.6 g/mL) obtained at 6 h (p.i.). [^{64}Cu]Cu-GluCAB-2^{Mal}-microPET/CT also provided information concerning the tracer uptake within the E0771 tumors (Figure 7C, marked T) presenting as a solid uniform mass on CT in all 4 scans; however, the PET signal intensity suggests a more heterogeneous tumor tissue distribution. In particular for PET signal intensity acquired at 1, 2 and 6 h followed a similar uptake pattern within the tumor tissue including areas of very low tracer presence - equal or less to the surrounding tissue (i.e. yielding T/NT ≤1.0) whereas other areas of the tumor can be clearly delineated from non-pathological tissue (any T/NT ≥1.0). This is not unexpected as the intratumoral distribution (over time) of [^{64}Cu]Cu-GluCAB-2^{Mal} markedly occurs due to the actual tumor microenvironment. It has been proposed that the diversity and degree of tumor perfusion depends on altered angiogenic responses to metabolic signals that normally regulate the structure of the blood distribution network. These abnormal responses may include addition of new microvessels in parallel to low resistance circuits and lengthening of existing microvessels in high resistance circuits. Hence,[48] tumor growth and perfusion are ultimately limited by the architecture of the existing arteriolar network. More importantly, this level of perfusion can also render the fate of delivery for drugs or radiopharmaceuticals in particular;[49] however [^{64}Cu]Cu-GluCAB-2^{Mal}-microPET/CT may be a valuable technique to visualize these alterations in tumor microenvironment also produced by EPR.

The tumor tissue expression as average SUV allowed illustrating E0771 tumor uptake quantification by way of time-activity-curves for [^{64}Cu]Cu-GluCAB-2^{Mal} which seemed approximately 4 times higher than for the control and 2 times higher than [^{64}Cu]Cu-GluCAB-1^{Mal}. Again, likely due to the heterogeneity of the PET signal intensity within each tumor and across the individual E0771 tumors/ group the only significant difference ($p = 0.01$ for [^{64}Cu]Cu-GluCAB-2^{NH2} and $p = 0.05$ for [^{64}Cu]Cu-GluCAB-1^{Mal}) was noted at 6 h p.i. The differences of the time-activity-curves comparing [^{64}Cu]Cu-GluCAB-2^{NH2} and [^{64}Cu]Cu-Glu-CAB-1^{Mal} were insignificant.

The tumor to muscle (T/M) ratio for [^{64}Cu]Cu-GluCAB-2^{Mal} in the first six hours averaged around 3.5 but increased to 4.8 after 24 hours; [^{64}Cu]Cu-GluCAB-1^{Mal} T/M ratio was 1.5 between 1 - 2 h and increased to 2.5 after 24 h; the total uptake of [^{64}Cu]Cu-GluCAB-2^{NH2} in the tumor was not high enough to delineate the tumor from surrounding tissue, such as muscle. [^{64}Cu]Cu-GluCAB-2^{Mal} therefore clearly demonstrated improved tumor accumulation over [^{64}Cu]Cu-GluCAB-1^{Mal}.

Post-mortem Biodistribution studies

The post-mortem/*ex vivo* biodistribution for [^{64}Cu]Cu-GluCAB-2^{NH2}, [^{64}Cu]Cu-GluCAB-1^{Mal} and [^{64}Cu]Cu-GluCAB-2^{Mal} was determined 24 h p.i. following the final microPET/CT image acquisition (Figure 8). The decay-corrected percentage activity residing in the organs was greatly reduced and correlated with the systemic clearance of the compounds as demonstrated by image-guided biodistribution. The maximum activity for [^{64}Cu]Cu-GluCAB-2^{NH2}was present in the large intestine (4.2 %ID/g), followed by the liver (3.2 %ID/g) with all other organs demonstrating < 2 %ID/g. The tumor presented with activity of

1.4 %ID/g. The maleimide compound, [^{64}Cu]Cu-GluCAB-2^{Mal}, indicated maximum activity remaining in the plasma (10.0 %ID/g) with half of that in the liver (5.0 %ID/g), tumor (4.6 %ID/g) and lungs (4.4 %ID/g). All other organs of mice administered with [^{64}Cu]Cu-GluCAB-2^{Mal} demonstrated < 3 %ID/g. Maximum activity presented in the liver and plasma of mice administered with [^{64}Cu]Cu-GluCAB-1^{Mal} (4.0 %ID/g and 3.9 %ID/g, respectively), followed by the large intestine (2.6 %ID/g) and all other organs (< 1.6 %ID/g). The average tumor activity for [^{64}Cu]Cu-GluCAB-1^{Mal} was only 0.9 %ID/g.

The significant difference ($p < 0.001$) between the activity remaining in the plasma of the maleimide compounds as compared to the amine-control compound is as a result of the binding of these compounds to albumin thereby prolonging the compound circulation time. In-line with the image-guided biodistribution, the activity in the liver of [^{64}Cu]Cu-GluCAB-2^{Mal} injected mice is approximately half of that remaining in the plasma while for [^{64}Cu]Cu-GluCAB-1^{Mal} the liver and plasma activity were approximately equal. This demonstrates the effectiveness of the GluCAB-2^{Mal} design to improve on liver clearance . The higher presence of activity in the organs of mice administered with [^{64}Cu]Cu-GluCAB-2^{Mal}, especially the well perfused organs, is as a result of the higher presence of the compound remaining in the blood. The activity remaining in the liver and large intestine for all three compounds is consistent with the identified hepatobiliary excretion for larger, more lipophilic complexes. The activity measured in the tumors after 24 h is consistent with the conclusions drawn from the microPET/CT images. Firstly, the tumor accumulation for [^{64}Cu]Cu-GluCAB-2^{NH_2} and [^{64}Cu]Cu-GluCAB-1^{Mal} is very low (< 1.5% ID/g) indicating minimal tumor targeting; and secondly, the increased tumor accumulation and targeting for [^{64}Cu]Cu-GluCAB-2^{Mal} is highly significant compared to the other compounds ($p < 0.05$) and to the muscle ($p < 0.001$). Visual examination of the excised tumors verified some heterogeneity to the tumors in terms of the amount of vascularization and location of blood pooling which would influence the standard deviation in the %ID/g for the tumors.

CONCLUSION

In light of the current and major concern to develop new radiopharmaceuticals and radioligands for diagnosis and therapy of diseases (theranostics), and given the fact that copper is a major player in this area thanks to its two radioisotopes,copper-64 and -67,offering access to both diagnostic and radiotherapeutic capabilities, we present here a second step in the development of a series of new, targeting theranostic agents for oncological purposes. The GluCAB derivative, GluCAB-2^{Mal} (tumor targeting based on *in vivo* binding to circulating albumin with tumor localization by the EPR effect as well as glucose metabolism) presented here, is designed to be an improvement on the first generation derivative, GluCAB-1^{Mal}, in terms of: ease and efficiency of synthesis; milder radiolabeling conditions; decreased liver accumulation and improved liver clearance; and demonstrated improved tumor targeting.

GluCAB-2^{Mal} was obtained following an efficient and improved synthesis procedure, as compared to the previous GluCAB-1^{Mal} via aTE3A-*C*-functionalised cyclam platform. Following the synthesis of GluCAB-2^{Mal}, the radiolabeling using copper-64 was completed to yield [^{64}Cu]Cu-GluCAB-2^{Mal} with a high labeling efficiency and radiochemical purity under physiological radiolabeling conditions making possible the future "kit" production for radiolabeling in clinics. *In vivo* analysis proved [^{64}Cu]Cu-GluCAB-2^{Mal} to have a comparable circulation time to [^{64}Cu]Cu-GluCAB-1^{Mal} but with superior liver metabolism and excretion, consistent with a negatively charged complex. Overall, it can be easily concluded that the aim of the improved design of this second generation GluCAB theranostic agent was realized and further works are in progress to adapt this GluCAB concept design for complexation with other copper radioisotopes and possibly other clinically useful radionuclides, leading to high performing, ready-to-label kits of new albumin-bioconjugate glucosyl theranostic agents.

EXPERIMENTAL SECTION

Material and methods

Reagents were purchased from ACROS Organics, TCI, ALDRICH Chemical Co. Compound **1** was synthesized as previously described(^{1}H and ^{13}C NMR spectra in ESI).[36] NMR data were recorded at the "Services communs" of the University of Brest. ^{1}H and ^{13}C NMR spectra were recorded with Bruker Avance 500 (500 MHz) or Bruker AMX-3 300 (300 MHz) spectrometers. The δ scales are relative to TMS (^{1}H, ^{13}C). The signals are indicated as follows: chemical shift, multiplicity (s, singlet; br s, broad singlet; d, doublet; t, triplet; m, multiplet), coupling constants J in hertz (Hz), assignment: CH_n-α-N or CH_n-β-N (n= 1 or 2) correspond to CH or CH_2 located in alpha or beta position of considered nitrogen atom, type of nuclei is indicated in italic; Ar is a generic term used in subscript for all H or C aromatic atoms; Ph is the abbreviation for C_6H_5 group, $PhNH_2$ corresponds to the aromatic group of the functionalization; Glu is an abbreviation for the glucosyl moiety; ano is attributed to H or C atoms in anomeric position; Bz corresponds to benzoyl group. HRMS spectra were recorded at the HRMS platform of the University of Orleans, France (FR 2708 CBM-ICOA).

All buffers and solutions used during radiolabelling were prepared according to standard methods using Milli-Q grade water (>18MΩ/cm). For investigation of ligand radiolabelling conditions,[^{64}Cu]$CuCl_2$ in 0.1M HCl (molar activity 115MBq/μmol) was obtained from the South African Nuclear Energy Corporation (Necsa). [^{64}Cu]$CuCl_2$ in 0.1M HCl (1GBq/mL) was kindly provided by RAPID Laboratory (Perth, Australia) for use during *in vivo* studies. [^{64}Cu]Cu-GluCAB-1^{Mal}, synthesized and radiolabeled as previously described,[23] was obtained from Radiochemistry Department, Necsa. *In vivo* studies were performed at the Nuclear Medicine Research Infrastructure (NuMeRI) – Pre-Clinical Imaging Facility (PCIF) based at Necsa. All radiolabelled solutions were purified using a Sep-Pak Light C-18 cartridge (Waters Corporation, Milford, MA, USA) pre-conditioned with EtOH (4 mL) and water (2 mL). Kit product vials were lyophilized using a Christ Alpha I-5, Type 1050 freeze-drier (*MedizinischeApparatebau*, *Harz*, Germany).

Experimental synthesis protocols and spectroscopic data of compounds

Compound 2

A solution of *tert*-butyl bromoacetate (443 mg, 2.27 mmol) in dry CH_3CN (2.5 mL) was added dropwise, over a period of 12h, to the suspension of compound **1** (321 mg, 0.81 mmol) and K_2CO_3 (560 mg, 4.05 mmol) in dry CH_3CN (20 mL) at -15°C. The solution was stirred 6 h after the completion of the addition. The mixture was then filtrated and the solvent was evaporated under reduced pressure. The crude product was purified by column chromatography on neutral aluminum oxide (CH_2Cl_2/MeOH 100:0 to 95:5) to afford compound **2** as a colorless oil (344 mg, 58%). ^{1}H NMR (300 MHz, $CDCl_3$, 25°C) δ 7.35-7.15 (m, 5H, C*H*$_{Ar}$Ph), 6.95 (d, *J* = 8.1 Hz,

2H, CH_{Ar}PhNH$_2$), 6.58 (d, J = 8.1 Hz, 2H, CH_{Ar}PhNH$_2$), 3.65-3.35 (m, 4H) 3.26 (s, 2H, CH_2-α-CO), 3.22(s, 2H, CH_2-α-CO) , 3.17 (s, 2H, CH_2-α-CO), 2.85-2.35 (m, 18H), 1.90 (m, 1H), 1.70-1.50 (m, 2H), 1.50-1.30 (m, 27H, CH_3). ^{13}C Jmod NMR (75 MHz, CDCl$_3$, 25°C) δ [171.4, 171.3, 171.1] (*C*O), [144.0, 140.0, 131.3] (*C*$_{Ar}$), 130.1 (CH_{Ar}PhNH$_2$), [128.9, 128.1, 126.7] (CH_{Ar}Ph), 115.1 (CH_{Ar} PhNH$_2$), [80.6, 80.5, 80.4] (*C*(CH$_3$)$_3$), [60.0, 57.8, 57.2, 51.7, 51.5, 51.2, 51.0 (×2), 50.9 (×2)] (*C*H$_2$-α-N), 39.3 (*C*H-β-N), 37.0 (*C*H$_2$PhNH$_2$), 28.3 (*C*H$_3$ ×9), 24.9 (*C*H$_2$-β-N). ESI-HRMS (positive) *m/z* calcd. for $[C_{42}H_{68}N_5O_6]^+$, 738.5164; found 738.5175 $[M+H]^+$.

Compound 3

Compound **2** (135 mg, 0.183 mmol) was dissolved in EtOH (20 mL) and palladium on activated charcoal 10% (0.200 g) was added to the solution. The mixture was stirred under a hydrogen atmosphere for 18 h. The mixture was filtrated through Celite® and the solvent was evaporated under reduced pressure to give compound **3** as a colorless oil (113 mg, 95%). ^{1}H NMR (300 MHz, CD$_3$CN, 25°C) δ 6.96 (d, J = 8.1 Hz, 2H, CH_{Ar} PhNH$_2$), 6.72 (d, J = 8.1 Hz, 2H, CH_{Ar} PhNH$_2$), 4.90 (br s, 2H, PhNH_2), 3.52-3.16 (m, 4H), 3.16-2.72 (m, 8 H), 2.72-2.48 (m, 5H), 2.47-2.19 (m, 5H), 2.19-1.98 (br s, 1H, N*H*), 1.85-1.58 (m, 3H), 1.58-1.28 (m, 28H). ^{13}C Jmod NMR (75 MHz, CD$_3$CN, 25°C) δ 170.5 (*C*O ×3), [144.3, 130.0] (*C*$_{Ar}$ PhNH$_2$), [129.7, 115.7] (*C*H$_{Ar}$ PhNH$_2$), [82.0, 81.5, 80.6] (*C*(CH$_3$)$_3$), [60.9, 60.7 (×2), 57.1, 56.3, 55.6, 54.1, 50.7, 49.3, 48.6, 46.6] (*C*H$_2$-α-N), 38.8 (*C*H$_2$PhNH$_2$), 38.7 (*C*H-β-N), 27.5 (*C*H$_3$ ×9), 22.7 (*C*H$_2$-β-N). ESI-HRMS (positive) *m/z* calcd. for $[C_{35}H_{62}N_5O_6]^+$, 648.4694; found 648.4693 $[M+H]^+$.

Compound 4

Glycosylated arm (125 mg, 0.153 mmol) in dry CH$_3$CN (2 mL) was added to the suspension of compound **3** (113 mg, 0.153 mmol) and K$_2$CO$_3$ (169 mg, 1.224 mmol) in dry CH$_3$CN (8 mL). The mixture was heated to reflux for 4 d. The mixture was then filtrated and the solvent was evaporated under reduced pressure. The crude product was purified by column chromatography on neutral aluminum oxide (CHCl$_3$/MeOH 100:0 to 95:5) to afford compound **4** as a colorless oil (144 mg, 68%). ^{1}H NMR (500 MHz, CDCl$_3$,25°C) δ 8.02 (d, J = 7.5 Hz, 2H, C*H*Bz), 7.96 (d, J = 7.0 Hz, 2H, C*H*Bz), 7.89 (d, J = 7.5 Hz, 2H, C*H*Bz), 7.82 (d, J = 7.0 Hz, 2H, C*H*Bz), 7.55-7.25 (m, 12H,C*H*Bz), 6.95 (d, J = 8.5 Hz, 2H,CH_{Ar} PhNH$_2$), 6.58 (d, J = 8.5 Hz, 2H, CH_{Ar} PhNH$_2$), 5.90 (t, J = 8.0 Hz, 1H, C*H*Glu), 5.67 (t, J = 8.0 Hz, 1H, C*H*Glu), 5.52 (dd, J = 9.5, 8.0 Hz, 1H, C*H*Glu), 4.83 (d, J = 8.0 Hz, 1H, CH_{ano}Glu), 4.63 (dd, J = 12.5, 3.5 Hz, 1H, CH_2OH Glu), 4.50 (dd, J = 12.5, 5.0 Hz, 1H, CH_2OH Glu), 4.15 (m, 1H, C*H*Glu), 3.90 (m, 1H, CH_2-OGlu), 3.53 (m, 3H, CH_2-OGlu (1H), PhNH_2), 3.30-3.15 (m, 6H, CH_2-α-CO ×3), 2.90-2.20 (m, 20H, CH$_2$-α-N + CH_2PhNH$_2$), 1.89 (m, 1H, C*H*β-N), 1.62-1.30 (m, 33H), 1.25-0.95 (m, 12H). ^{13}C Jmod NMR (125 MHz, CDCl$_3$, 25°C) δ [171.3 (×2), 171.1, 166.2, 165.8, 165.2, 165.1] (*C*O), 143.9 (*C*$_{Ar}$PhNH$_2$), [133.4, 133.2, 133.1, 133.1] (*C*H$_{Ar}$Bz), 131.3 (*C*$_{Ar}$PhNH$_2$), 130.0 (*C*H$_{Ar}$ PhNH$_2$), [129.83, 129.77 (x3)] (*C*H$_{Ar}$Bz), [129.6, 129.4, 128.8 (×2)] (*C*$_{Ar}$Bz), [128.4, 128.35 (×2), 128.29] (*C*H$_{Ar}$Bz), 115.1 (*C*H$_{Ar}$ PhNH$_2$), 101.3 (*C*H$_{ano}$Glu), 80.6 (*C*(CH$_3$)$_3$ (×3)), [72.9, 72.2, 71.9] (*C*H Glu), 70.4 (CH$_2$-α-OGlu), 69.9 (*C*HGlu), 63.3 (*C*H$_2$-OBz), [58.2, 57.93, 57.87, 57.79, 57.3, 55.9, 51.7, 51.6, 51.2 (×3), 50.8] (*C*H$_2$-α-N), 39.3 (*C*H-β-N), 37.0 (*C*H$_2$PhNH$_2$), [29.7, 29.6, 29.5, 29.4, 29.2] (*C*H$_2$ fatty chain), 28.2 (*C*H$_3$×9), [27.6, 27.5, 25.8] (*C*H$_2$ fatty chain), 24.8 (*C*H$_2$-β-N). ESI-HRMS (positive) *m/z* calcd. for $[C_{79}H_{108}N_5O_{16}]^+$, 1382.7785; found 1382.7782 $[M+H]^+$.

Compound GluCAB-2^{NH2}

Compound **4** (209 mg, 0.151 mmol) was dissolved in 2 mL of a mixture of aqueous KOH (1M) and EtOH (1:1). The solution was heated to 80°C for 20 h. The solvent was evaporated under pressure and the crude product was purified by a reverse phase C18 HPLC-chromatography (H$_2$O/CH$_3$CN from 0 to 80% of CH$_3$CN). Fractions were collected and lyophilized to give compound GluCAB-2^{NH2} under its potassium salt as a white powder (69 mg, 0.076 mmol, 50%). ^{1}H NMR (500 MHz, D$_2$O, 25°C) δ 7.08 (d, J = 8.4 Hz, 2H, CH_{Ar} PhNH$_2$), 6.82 (d, J = 8.4 Hz, 2H, CH_{Ar} PhNH$_2$), 4.45 (d, 1H, J = 8.0 Hz, CH_{ano}), 3.98-3.83 (m, 2H, CH$_2$-α-OGlu), 3.74-3.62 (m, 3H), 3.55 (d, J = 16.7 Hz, 1H), 3.49 (d, J = 9.1 Hz, 1H), 3.47-3.41 (m, 2H), 3.41-3.35 (m, 2H), 3.34 (s, 2H), 3.30-3.19 (m, 6H), 3.19-3.04 (m, 7H), 2.95 (m, 3H), 2.78 (s, 1H), 2.66 (s, 3H), 2.50 (m, 2H), 2.40 (br s, 1H), 2.05 (br s, 1H) 1.80-1.50 (m, 5H), 1.39-1.24 (m, 12H). ^{13}C Jmod NMR (125 MHz, D$_2$O, 25°C) δ 182.0 (*C*O ×3), 147.5 (*C*$_{Ar}$Ph), 132.9 (*C*H$_{Ar}$ PhNH$_2$), 132.2 (*C*$_{Ar}$Ph), 119.5 (*C*H$_{Ar}$ PhNH$_2$), 105.0 (*C*H$_{ano}$Glu), [78.7 (×2), 76.0] (*C*H Glu), 74.0 (*C*H$_2$-α-OGlu), 73.5(*C*H Glu), 63.6 (*C*H$_2$OHGlu), [56.2-38.4] (coalescence phenomenon in the range of *C*H$_2$-α-N and *C*H-α-N signals), [31.6, 31.3, 31.2, 31.2, 30.9, 28.6, 27.9] (*C*H$_2$ fatty chain), 23.7 (*C*H$_2$-β-N). ESI-HRMS(positive) *m/z* calcd. for $[C_{39}H_{68}N_5O_{12}]^+$, 798.4859; found 798.4842 $[M+4H]^+$.

General procedure for ^{64}Cu-labeling ofGluCAB-2^{NH2}

In NH$_4$OAc Buffer: A solution of[^{64}Cu]CuCl$_2$ (20μL, 0.4 equiv, 20-40 MBq) was added to a solution of GluCAB-2^{NH2} (1 equiv) in NH$_4$OAc buffer (50 μL, 0.1 M) and Milli-Q H$_2$O (30 μL). The pH was adjusted to 3.5 by addition of NaOH (2 M) and HCl (0.6 M) and the reaction was heated for 30 min at 90°C. The solution was then purified by C18 cartridge and dried under argon.

In PBS Buffer: A solution of[^{64}Cu]CuCl$_2$ (20 μL 0.4 equiv, 20-40 MBq) was added to a solution of GluCAB-2^{NH2} (1 equiv) in PBS buffer (80 μL, 0.01 M) The reaction was then heated 20 min at 45°C. The solution was then purified by C18 cartridge and dried under argon.

Maleimide coupling reaction and synthesis of [^{64}Cu]Cu-Glu-CAB-2^{Mal}

Method A – Post-labeling conversion: A solution of[^{64}Cu]CuCl$_2$ (25.3 μL, 25.3 MBq, 0.4 equiv) was added to a solution of GluCAB-2^{NH2} (0.70 mg, 0.87 μmol) in NH$_4$OAc buffer (50 μL, 0.1 M) and Milli-Q H$_2$O (25 μL). The pH was adjusted to 3.5 by addition of NaOH (2 M) and HCl (0.6 M) and the reaction was heated 30 min at 90°C. The solution was then purified by C18 cartridge and dried under argon. The residue was dissolved in PBS (200 μL, 0.01M) and 4-Maleimidobutyric acid-*N*-hydroxysuccinimide ester(0.442 mg, 2 equiv) solubilized in DMF (4.42 μL) was added to the solution. The reaction was stirred 1h15 at 25°C, purified by C18 cartridge and dried under argon. The residue was dissolved in PBS buffer (180 μL, 0.01 M) and the radiochemical purity was evaluated by radio-HPLC.

Method B – Pre-labeling conversion: 4-Maleimidobutyic acid-*N*-hydroxysuccinimide ester (1.88 mg, 6.70 μmol,5 equiv) solubilized in DMF (18.8 μL) was added to a solution of GluCAB-2^{NH2}(0.72 mg, 1.34 μmol) in a PBS buffer (381.2 μL, 0.01 M, pH 7.4). The solution was stirred 1h30 at 45°C. The solvent was then evaporated under air flow. The residue was then solubilized in PBS buffer (171.9 μL, 0.01 M, pH 7.4) and the solution of [^{64}Cu]CuCl$_2$ (28.1 μL, 28.1 MBq, 0.4 equiv) was added. The reaction was heated at 45 °C for 30 min then filtered and purified by C18 cartridge. The solvent was evaporated under air flow. The residue was dissolved in PBS buffer (200 μL, 0.01 M) and the radiochemical purity was evaluated by radio-HPLC.

General procedure for "ready-to-label" GluCAB-2^{Mal} kit

4-Maleimidobutyic acid-N-hydroxysuccinimide ester (5 equiv) was solubilized in a small volume of DMF and added to a solution of GluCAB-2^{NH2} (1 equiv) in a PBS buffer (400 μL, 0.01 M, pH

7.4). The solution was stirred for 90 min at 45°C and then purified by C18 cartridge. The solution was dried under argon and redissolved in PBS buffer (0.01 M, pH 7.4). The solution was then divided in several vials (150 to 600 µg of GluCAB-2^{Mal} per vial) and lyophilized.

In vitro stability tests

EDTA transchelation assay

The stability of the radiolabelled metal-chelator complex was determined by evaluating the transchelation of [^{64}Cu]Cu-Glu-CAB-2^{NH2} with ethylenediaminetetraacetic acid (EDTA) according to a previously described method.[50] The radiolabelled compound (10 µL, 5 MBq) was diluted with 0.01 M PBS (890 µL, pH 7) and 0.05 M EDTA (100 µL, 25 equiv) added. After shaking briefly, the mixture was incubated at room temperature with a sample (50 µL) being drawn at 10, 60 and 120 min for radio-HPLC analysis (conditions as described).

Protein Binding and Serum Stability

The serum protein binding and stability of [^{64}Cu]Cu-GluCAB-1^{Mal} was previously reported.[23] The serum protein binding and stability of [^{64}Cu]Cu-GluCAB-2^{NH2} and [^{64}Cu]Cu-GluCAB-2^{Mal} was evaluated according to the method as described.[51] Briefly, the desired radiolabelled compound ([^{64}Cu]Cu-GluCAB-2^{NH2} (50 µL, ~ 3 MBq) or [^{64}Cu]Cu-GluCAB-2^{Mal} (50 µL, ~ 1 MBq) was added to serum (450 µL) at 37 °C and incubated over 24 h. Serum samples (100 µL) were drawn at 0, 1, 2 and 24 h after addition of the compound. Serum proteins were precipitated by addition of cold acetonitrile (500 µL) followed by centrifuging for 5 min at 6000 rpm (Hettich EBA 20; A. *Hettich GmbH* & Co, Tuttlingen, *Germany)*. The supernatant was withdrawn and the protein pellet was washed with acetonitrile (100 µL). For protein binding analysis, the activity of the pellet and supernatant (combined with the wash) was measured using automated gamma counting (*Hidex AMG LabLogic, Turku, Finland).* All measured activities were decay-corrected and the protein binding expressed as a percentage of the total activity measured. The protein binding studies were done in triplicate and the data reported as the mean ± standard deviation (SD). For serum stability, the supernatant of the sample was diluted with MilliQ water (500 µL) and analyzed by radio-HPLC (conditions as described).

In vivo and *ex vivo* studies

Radiolabeling of GluCAB-2^{Mal} kit for in vivo studies

GluCAB-2^{Mal} (150 µg, 174 nmol) ("150 µg kit") was solubilized in Milli-Q H_2O (25 µL) and then PBS buffer (125 µL, 0.01 M, pH 7.4) was added. The solution of [^{64}Cu]$CuCl_2$ in HCl 0.1M 100 µL, 100 MBq) was added and the pH adjusted to 7.4 with a solution of NaOH (2 M). The reaction was heated 30 min at 45 °C and then purified by C18 cartridge. The solvent was evaporated under air flow and solubilized again in PBS buffer (750 µL, 0.01 M, pH 7.4) for *in vivo* injection.

In vivo characterization of [^{64}Cu]Cu-GluCAB-1^{Mal}, [^{64}Cu]Cu-Glu-CAB-2^{NH2} and [^{64}Cu]Cu-GluCAB-2^{Mal}

Ethical approval for the *in vivo* study was gained from the North West University Animal Research Ethics Committee (NWU-AnimCareREC) and conducted in accordance with the South African guidelines – SANS 10386: The use of laboratory animals for research purposes.

Animal preparation and compound administration: Allograft E0771 breast cancer C57/BL6 mice (female, 6-8 weeks, 16 – 20 g; inoculated in the upper mammary fat with 1 x 10^6 cells; average tumor volume of 291 ± 91 mm^3) were obtained from the Pre-Clinical Drug Development Platform (PCDDP) Vivarium, North West University (Potchefstroom, SA) and allowed a 7-day acclimatisation period before commencement of study. The mice (n = 5 per group) were administered intravenously into the tail vein with 0.1 - 0.15 mL of the compounds as follows: [^{64}Cu]Cu-GluCAB-1^{Mal} 9.18 MBq ± 0.42 (0.49 MBq/g mouse), [^{64}Cu]Cu-GluCAB-2^{NH2} 10.84 MBq ± 6.00 (0.62 MBq/g mouse) and [^{64}Cu]Cu-Glu-CAB-2^{Mal} 7.21 MBq ± 0.77 (0.40 MBq/g mouse). The animals were anaesthetized for microPET/CT imaging using isoflurane in oxygen (3 - 4% for induction and 2 – 2.5% for maintenance).

MicroPET/CT image acquisition, reconstruction and data quantification: Functional molecular imaging of the 3 out of 5 injected mice per group was performed using a small animal PET/CT camera (NanoScan PET/CT, Mediso Medical Imaging Systems, Budapest, Hungary) at 1, 2, 6 and 24 h post-injection. Animals were placed in the prone-head first position. CT XRay scans were completed as follows: 300 s, 360 projections in semi-circular mode, max FOV, binning – 1:4, Reconstruction (Nucline software (Mediso Ltd, Budapest, Hungary)): medium voxel size, medium slice-thickness, cosine filter. PET images were acquired using the following settings: 20 min, 1-bed position and reconstruction completed using list mode: 3D OSEM, coincidence mode – 1-5 with detector normalization and corrections for random events. Coregistered PET/CT images in the axial, coronal and sagittal orientation as well as maximum intensity projections (MIP) were visualized and analyzed using InterView Fusion software (Mediso Ltd, Budapest, Hungary). The images were normalized (low 0.0; high 4.0) to allow for comparison between different time points and between the three compounds. Semi-quantification of the activity in the organs was obtained through 3D-volumes of interest (VOI) drawn around the specified area and expressed as the mean standardized uptake value (SUV) (g/mL). These values were used to generate image-guided time-activity-curves for compound biodistribution in the organs over the 24h period.

Ex vivo biodistribution of [^{64}Cu]Cu-GluCAB-1^{Mal}, [^{64}Cu]Cu-Glu-CAB-2^{NH2} and [^{64}Cu]Cu-GluCAB-2^{Mal}

After completion of the final image acquisition at 24 h p.i, for the [^{64}Cu]Cu-GluCAB compounds, the animals were euthanized by anesthesia overdose followed by decapitation. Blood was immediately collected into a pre-weighed serum separator tube (SST-Vacutainer)(Becton, Dickinson and Company, Franklin Lakes, NJ, USA) and the serum separated by centrifugation (5 min; 6000 rpm; Hettich EBA 20; A. *Hettich GmbH* & Co, Tuttlingen, *Germany)*. The animals were dissected, organs collected (pre-weighed plastic vials) and all samples measured using an *automatic gamma counter* (*Hidex AMG LabLogic, Turku, Finland)*. The counts/MBq, for correlation of the injected dose activity to the activity measured on the HIDEX, was determined using a standard dilution of ^{64}Cu-activity (100, 200 and 500 µL). This value was then used to express the organ activity as a decay-corrected, percentage of the injected dose per gram of tissue (%ID/g).

ASSOCIATED CONTENT

Supporting Information

The Supporting Information is available free of charge at https://....

. Characterization of the compounds and complexes synthesized (^{1}H, ^{13}C, ESI-HRMS, analytical HPLC)

AUTHOR INFORMATION

Corresponding Authors

Prof. Raphael Tripier: raphael.tripier@univ-brest.fr
Dr Nathalie Le Bris: nathalie.lebris@univ-brest.fr
Dr Jan Rijn Zeevaart: janrijn.zeevaart@necsa.co.za

Author Contributions

The manuscript was written through contributions of all authors. All authors have given approval to the final version of the manuscript.

Conflicts of interest

There are no conflicts to declare

ACKNOWLEDGMENT

R.T. and N.L.B. acknowledge the Ministère de l'Enseignement Supérieur et de la Recherche, the Centre National de la Recherche Scientifique and in particular "La Ligue contre le Cancer" for the PhD fellowship of T.L.B. The University of Brest and NECSA for co-funding its three months period mission in Pretoria in NECSA company installations. R.T. and N.L.B. also thanks the "Service Commun" NMR facilities of the University of Brest.

Necsa authors acknowledge financial and infrastructure support provided by BGM Pharmaceuticals, South Africa and the Nuclear Medicine Research Infrastructure (NuMeRI) NPO as funded by the Department of Science and Innovation (DSI), South Africa.

Thanks go to the staff at the Pre-Clinical Drug Development Platform (PCDDP), NWU, Potchefstroom for assistance with *in vivo* studies and associated LAT/Veterinary services as well as to Ms D van Wyk (Steve Biko Academic Hospital, Nuclear Medicine) for assistance during microPET/CT imaging.

REFERENCES

(1) Condeelis, J.; Weissleder, R. In Vivo Imaging in Cancer. *Cold Spring Harb. Perspect. Biol.* **2010**, *2* (12). https://doi.org/10.1101/cshperspect.a003848.

(2) Marcus, C.; Mena, E.; Subramaniam, R. M. Brain Pet in the Diagnosis of Alzheimer's Disease. *Clin. Nucl. Med.* **2014**, *39* (10). https://doi.org/10.1097/RLU.0000000000000547.

(3) Kumar, V.; Boddeti, D. K. 68Ga-Radiopharmaceuticals for PET Imaging of Infection and Inflammation. In *Theranostics, Gallium-68, and Other Radionuclides*; Baum, R. P., Rösch, F., Eds.; Recent Results in Cancer Research; Springer: Berlin, Heidelberg, 2013; pp 189–219. https://doi.org/10.1007/978-3-642-27994-2_11.

(4) Lopci, E.; Grassi, I.; Chiti, A.; Nanni, C.; Cicoria, G.; Toschi, L.; Fonti, C.; Lodi, F.; Mattioli, S.; Fanti, S. PET Radiopharmaceuticals for Imaging of Tumor Hypoxia: A Review of the Evidence. *Am. J. Nucl. Med. Mol. Imaging* **2014**, *4* (4), 365–384.

(5) Evans, N. R.; Tarkin, J. M.; Chowdhury, M. M.; Warburton, E. A.; Rudd, J. H. F. PET Imaging of Atherosclerotic Disease: Advancing Plaque Assessment from Anatomy to Pathophysiology. *Curr. Atheroscler. Rep.* **2016**, *18* (6), 30. https://doi.org/10.1007/s11883-016-0584-3.

(6) Kim, J.; Park, J. E.; Nahrendorf, M.; Kim, D.-E. Direct Thrombus Imaging in Stroke. *J. Stroke* **2016**, *18* (3), 286–296. https://doi.org/10.5853/jos.2016.00906.

(7) Rahmim, A.; Zaidi, H. PET versus SPECT: Strengths, Limitations and Challenges. *Nucl. Med. Commun.* **2008**, *29* (3), 193–207. https://doi.org/10.1097/MNM.0b013e3282f3a515.

(8) Le Bars, D. Fluorine-18 and Medical Imaging: Radiopharmaceuticals for Positron Emission Tomography. *J. Fluor. Chem.* **2006**, *127* (11), 1488–1493. https://doi.org/10.1016/j.jfluchem.2006.09.015.

(9) Ramogida, C. F.; Orvig, C. Tumour Targeting with Radiometals for Diagnosis and Therapy. *Chem. Commun. Camb. Engl.* **2013**, *49* (42), 4720–4739. https://doi.org/10.1039/c3cc41554f.

(10) Kraeber-Bodéré, F.; Rousseau, C.; Bodet-Milin, C.; Mathieu, C.; Guérard, F.; Frampas, E.; Carlier, T.; Chouin, N.; Haddad, F.; Chatal, J.-F.; Faivre-Chauvet, A.; Chérel, M.; Barbet, J. Tumor Immunotargeting Using Innovative Radionuclides. *Int. J. Mol. Sci.* **2015**, *16* (2), 3932–3954. https://doi.org/10.3390/ijms16023932.

(11) Maeda, H.; Tsukigawa, K.; Fang, J. A Retrospective 30 Years After Discovery of the Enhanced Permeability and Retention Effect of Solid Tumors: Next-Generation Chemotherapeutics and Photodynamic Therapy—Problems, Solutions, and Prospects. *Microcirculation* **2016**, *23* (3), 173–182. https://doi.org/10.1111/micc.12228.

(12) Maeda, H.; Wu, J.; Sawa, T.; Matsumura, Y.; Hori, K. Tumor Vascular Permeability and the EPR Effect in Macromolecular Therapeutics: A Review. *J. Controlled Release* **2000**, *65* (1–2), 271–284. https://doi.org/10.1016/S0168-3659(99)00248-5.

(13) Maeda, H.; Nakamura, H.; Fang, J. The EPR Effect for Macromolecular Drug Delivery to Solid Tumors: Improvement of Tumor Uptake, Lowering of Systemic Toxicity, and Distinct Tumor Imaging in Vivo. *Adv. Drug Deliv. Rev.* **2013**, *65* (1), 71–79. https://doi.org/10.1016/j.addr.2012.10.002.

(14) Kue, C. S.; Kamkaew, A.; Burgess, K.; Kiew, L. V.; Chung, L. Y.; Lee, H. B. Small Molecules for Active Targeting in Cancer. *Med. Res. Rev.* **2016**, *36* (3), 494–575. https://doi.org/10.1002/med.21387.

(15) Heiden, M. G. V.; Cantley, L. C.; Thompson, C. B. Understanding the Warburg Effect: The Metabolic Requirements of Cell Proliferation. *Science* **2009**, *324* (5930), 1029–1033. https://doi.org/10.1126/science.1160809.

(16) Macheda, M. L.; Rogers, S.; Best, J. D. Molecular and Cellular Regulation of Glucose Transporter (GLUT) Proteins in Cancer. *J. Cell. Physiol.* **2005**, *202* (3), 654–662. https://doi.org/10.1002/jcp.20166.

(17) Medina, R. A.; Owen, G. I. Glucose Transporters: Expression, Regulation and Cancer. *Biol. Res.* **2002**, *35* (1), 9–26. https://doi.org/10.4067/S0716-97602002000100004.

(18) Weber, J.; Bollepalli, L.; Belenguer, A. M.; Antonio, M. D.; Mitri, N. D.; Joseph, J.; Balasubramanian, S.; Hunter, C. A.; Bohndiek, S. E. An Activatable Cancer-Targeted Hydrogen Peroxide Probe for Photoacoustic and Fluorescence Imaging. *Cancer Res.* **2019**, *79* (20), 5407–5417. https://doi.org/10.1158/0008-5472.CAN-19-0691.

(19) Li, Z.; Conti, P. S. Radiopharmaceutical Chemistry for Positron Emission Tomography. *Adv. Drug Deliv. Rev.* **2010**, *62* (11), 1031–1051. https://doi.org/10.1016/j.addr.2010.09.007.

(20) Novak-Hofer, I.; Schubiger, A. P. Copper-67 as a Therapeutic Nuclide for Radioimmunotherapy. *Eur. J. Nucl. Med. Mol. Imaging* **2002**, *29* (6), 821–830. https://doi.org/10.1007/s00259-001-0724-y.

(21) Wadas, T. J.; Wong, E. H.; Weisman, G. R.; Anderson, C. J. Coordinating Radiometals of Copper, Gallium, Indium, Yttrium, and Zirconium for PET and SPECT Imaging of Disease. *Chem. Rev.* **2010**, *110* (5), 2858–2902. https://doi.org/10.1021/cr900325h.

(22) Price, E. W.; Orvig, C. Matching Chelators to Radiometals for Radiopharmaceuticals. *Chem. Soc. Rev.* **2013**, *43* (1), 260–290. https://doi.org/10.1039/C3CS60304K.

(23) Driver, C. H. S.; Ebenhan, T.; Zeevaart, J. R.; Hunter, R.; Parker, I.; Szucs, Z. Towards the Development of a Targeted Albumin-Binding Radioligand for Theranostic Applications: Synthesis, Radiolabelling and Preliminary In Vivo Studies. **2020**. https://doi.org/10.26434/chemrxiv.12687920.v1.

(24) Kratz, F. Albumin as a Drug Carrier: Design of Prodrugs, Drug Conjugates and Nanoparticles. *J. Controlled Release* **2008**, *132* (3), 171–183. https://doi.org/10.1016/j.jconrel.2008.05.010.

(25) Liu, Z.; Chen, X. Simple Bioconjugate Chemistry Serves Great Clinical Advances: Albumin as a Versatile Platform for Diagnosis and Precision Therapy. *Chem. Soc. Rev.* **2016**, *45* (5), 1432–1456. https://doi.org/10.1039/C5CS00158G.

(26) Lau, J.; Jacobson, O.; Niu, G.; Lin, K.-S.; Bénard, F.; Chen, X. Bench to Bedside: Albumin Binders for Improved Cancer Radioligand Therapies. *Bioconjug. Chem.* **2019**, *30* (3), 487–502. https://doi.org/10.1021/acs.bioconjchem.8b00919.

(27) E, M.; Gp, S.; F, T.; S, T. Albumin-Bound Formulation of Paclitaxel (Abraxane ABI-007) in the Treatment of Breast Cancer. *Int. J. Nanomedicine* **2009**, *4*, 99–105. https://doi.org/10.2147/ijn.s3061.

(28) Thom, V. J.; Hosken, G. D.; Hancock, R. D. Anomalous Metal Ion Size Selectivity of Tetraaza Macrocycles. *Inorg. Chem.* **1985**, *24* (21), 3378–3381. https://doi.org/10.1021/ic00215a017.

(29) Hancock, R. D. Molecular Mechanics Calculations and Metal Ion Recognition. *Acc. Chem. Res.* **1990**, *23* (8), 253–257. https://doi.org/10.1021/ar00176a003.

(30) Navarro, A.-S.; Le Bihan, T.; Le Saëc, P.; Le Bris, N.; Bailly, C.; Saï-Maurel, C.; Bourgeois, M.; Chérel, M.; Tripier, R.; Faivre-Chauvet, A. TE1PA as Innovating Chelator for 64Cu Immuno-TEP Imaging: A Comparative in Vivo Study with DOTA/NOTA by Conjugation on 9E7.4 MAb in a Syngeneic Multiple Myeloma Model. *Bioconjug. Chem.* **2019**, *30* (9), 2393–2403. https://doi.org/10.1021/acs.bioconjchem.9b00510.

(31) Wieser, G.; Mansi, R.; Grosu, A. L.; Schultze-Seemann, W.; Dumont-Walter, R. A.; Meyer, P. T.; Maecke, H. R.; Reubi, J. C.; Weber, W. A. Positron Emission Tomography (PET) Imaging of Prostate Cancer with a Gastrin Releasing Peptide Receptor Antagonist - from Mice to Men. *Theranostics* **2014**, *4* (4), 412–419. https://doi.org/10.7150/thno.7324.

(32) Bailly, C.; Gouard, S.; Guérard, F.; Chalopin, B.; Carlier, T.; Faivre-Chauvet, A.; Remaud-Le Saëc, P.; Bourgeois, M.; Chouin, N.; Rbah-Vidal, L.; Tripier, R.; Haddad, F.; Kraeber-Bodéré, F.; Bodet-Milin, C.; Chérel, M. What Is the Best Radionuclide for Immuno-PET of Multiple Myeloma? A Comparison Study Between 89Zr- and 64Cu-Labeled Anti-CD138 in a Preclinical Syngeneic Model. *Int. J. Mol. Sci.* **2019**, *20* (10), 2564. https://doi.org/10.3390/ijms20102564.

(33) Sprague, J. E.; Peng, Y.; Sun, X.; Weisman, G. R.; Wong, E. H.; Achilefu, S.; Anderson, C. J. Preparation and Biological Evaluation of Copper-64–Labeled Tyr3-Octreotate Using a Cross-Bridged Macrocyclic Chelator. *Clin. Cancer Res.* **2004**, *10* (24), 8674–8682. https://doi.org/10.1158/1078-0432.CCR-04-1084.

(34) Pandya, D. N.; Kim, J. Y.; Kwak, W.; Park, J. C.; Gawande, M. B.; An, G. I.; Ryu, E. K.; Yoo, J. A New Synthesis of TE2A—a Potential Bifunctional Chelator for 64Cu. *Nucl. Med. Mol. Imaging* **2010**, *44* (3), 185–192. https://doi.org/10.1007/s13139-010-0031-2.

(35) Cai, Z.; Ouyang, Q.; Zeng, D.; Nguyen, K. N.; Modi, J.; Wang, L.; White, A. G.; Rogers, B. E.; Xie, X.-Q.; Anderson, C. J. 64Cu-Labeled Somatostatin Analogues Conjugated with Cross-Bridged Phosphonate-Based Chelators via Strain-Promoted Click Chemistry for PET Imaging: In Silico through in Vivo Studies. *J. Med. Chem.* **2014**, *57* (14), 6019–6029. https://doi.org/10.1021/jm500416f.

(36) Pandya, D. N.; Kim, J. Y.; Park, J. C.; Lee, H.; Phapale, P. B.; Kwak, W.; Choi, T. H.; Cheon, G. J.; Yoon, Y.-R.; Yoo, J. Revival of TE2A; a Better Chelate for Cu(II) Ions than TETA? *Chem. Commun.* **2010**, *46* (20), 3517–3519. https://doi.org/10.1039/B925703A.

(37) DRIVER, C. H. S.; Zeevaart, J. R.; Parker, M. I.; Hunter, R. Radiopharmaceutical Conjugate. US20170296684A1, October 19, 2017.

(38) Jones-Wilson, T. M.; Deal, K. A.; Anderson, C. J.; McCarthy, D. W.; Kovacs, Z.; Motekaitis, R. J.; Sherry, A. D.; Martell, A. E.; Welch, M. J. The in Vivo Behavior of Copper-64-Labeled Azamacrocyclic Complexes. *Nucl. Med. Biol.* **1998**, *25* (6), 523–530. https://doi.org/10.1016/S0969-8051(98)00017-1.

(39) Camus, N.; Halime, Z.; Le Bris, N.; Bernard, H.; Platas-Iglesias, C.; Tripier, R. Full Control of the Regiospecific N-Functionalization of C-Functionalized Cyclam Bisaminal Derivatives and Application to the Synthesis of Their TETA, TE2A, and CB-TE2A Analogues. *J. Org. Chem.* **2014**, *79* (5), 1885–1899. https://doi.org/10.1021/jo4028566.

(40) Halime, Z.; Frindel, M.; Camus, N.; Orain, P.-Y.; Lacombe, M.; Chérel, M.; Gestin, J.-F.; Faivre-Chauvet, A.; Tripier, R. New Synthesis of Phenyl-Isothiocyanate C-Functionalised Cyclams. Bioconjugation and 64Cu Phenotypic PET Imaging Studies of Multiple Myeloma with the Te2a Derivative. *Org. Biomol. Chem.* **2015**, *13* (46), 11302–11314. https://doi.org/10.1039/C5OB01618E.

(41) Le Bihan, T.; Navarro, A.-S.; Le Bris, N.; Le Saëc, P.; Gouard, S.; Haddad, F.; Gestin, J.-F.; Chérel, M.; Faivre-Chauvet, A.; Tripier, R. Synthesis of C-Functionalized TE1PA and Comparison with Its Analogues. An Example of Bioconjugation on 9E7.4 MAb for Multiple Myeloma 64Cu-PET Imaging. *Org. Biomol. Chem.* **2018**, *16* (23), 4261–4271. https://doi.org/10.1039/C8OB00499D.

(42) Murakami, T.; Sato, Y.; Shibakami, M. Stereoselective Glycosylations Using Benzoylated Glucosyl Halides with Inexpensive Promoters. *Carbohydr. Res.* **2008**, *343* (8), 1297–1308. https://doi.org/10.1016/j.carres.2008.03.019.

(43) Murphy, J. Pre-Clinical Murine Models: Syngeneic Models for Immuno-Oncology. *MOJ Immunol.* **2015**, *2* (4). https://doi.org/10.15406/moji.2015.02.00052.

(44) Jong, M. de; Maina, T. Of Mice and Humans: Are They the Same?—Implications in Cancer Translational Research. *J. Nucl. Med.* **2010**, *51* (4), 501–504. https://doi.org/10.2967/jnumed.109.065706.

(45) Yang, Y.; Yang, H. H.; Hu, Y.; Watson, P. H.; Liu, H.; Geiger, T. R.; Anver, M. R.; Haines, D. C.; Martin, P.; Green, J. E.; Lee, M. P.; Hunter, K. W.; Wakefield, L. M. Immunocompetent Mouse Allograft Models for Development of Therapies to Target Breast Cancer Metastasis. *Oncotarget* **2017**, *8* (19), 30621–30643. https://doi.org/10.18632/oncotarget.15695.

(46) Yang, D.-Q.; Freund, D. M.; Harris, B. R. E.; Wang, D.; Cleary, M. P.; Hegeman, A. D. Measuring Relative Utilization of Aerobic Glycolysis in Breast Cancer Cells by Positional Isotopic Discrimination. *FEBS Lett.* **2016**, *590* (18), 3179–3187. https://doi.org/10.1002/1873-3468.12360.

(47) Lim, S.; Hosaka, K.; Nakamura, M.; Cao, Y. Co-Option of Pre-Existing Vascular Beds in Adipose Tissue Controls Tumor Growth Rates and Angiogenesis. *Oncotarget* **2016**, *7* (25), 38282–38291. https://doi.org/10.18632/oncotarget.9436.

(48) Gillies, R. J.; Schomack, P. A.; Secomb, T. W.; Raghunand, N. Causes and Effects of Heterogeneous Perfusion in Tumors. *Neoplasia* **1999**, *1* (3), 197–207. https://doi.org/10.1038/sj.neo.7900037.

(49) Stylianopoulos, T.; Munn, L. L.; Jain, R. K. Reengineering the Physical Microenvironment of Tumors to Improve Drug Delivery and Efficacy: From Mathematical Modeling to Bench to Bedside. *Trends Cancer* **2018**, *4* (4), 292–319. https://doi.org/10.1016/j.trecan.2018.02.005.

(50) Qin, Z.; Hoh, C. K.; Hall, D. J.; Vera, D. R. A Tri-Modal Molecular Imaging Agent for Sentinel Lymph Node Mapping. *Nucl. Med. Biol.* **2015**, *42* (12), 917–922. https://doi.org/10.1016/j.nucmedbio.2015.07.011.

(51) Beaino, W.; Anderson, C. J. PET Imaging of Very Late Antigen-4 in Melanoma: Comparison of 68Ga- and 64Cu-Labeled NODAGA and CB-TE1A1P-LLP2A Conjugates. *J. Nucl. Med.* **2014**, *55* (11), 1856–1863. https://doi.org/10.2967/jnumed.114.144881.

TOC Graphic